IOPscience iopscience.iop.org

Home Search Collections Journals About Contact us My IOPscience

Influence of indium concentration and substrate temperature on the physical characteristics of chemically sprayed ZnO:In thin films deposited from zinc pentanedionate and indium sulfate

This article has been downloaded from IOPscience. Please scroll down to see the full text article.

2006 J. Phys.: Condens. Matter 18 5105

(http://iopscience.iop.org/0953-8984/18/22/010)

View the table of contents for this issue, or go to the journal homepage for more

Download details:
IP Address: 129.252.86.83
The article was downloaded on 28/05/2010 at 11:07

Please note that terms and conditions apply.

INSTITUTE OF PHYSICS PUBLISHING JOURNAL OF PHYSICS: CONDENSED MATTER

J. Phys.: Condens. Matter **18** (2006) 5105–5120 doi:10.1088/0953-8984/18/22/010

Influence of indium concentration and substrate temperature on the physical characteristics of chemically sprayed ZnO:In thin films deposited from zinc pentanedionate and indium sulfate

L Castañeda[1], O G Morales-Saavedra[1,4], J C Cheang-Wong[2], D R Acosta[2], J G Bañuelos[1], A Maldonado[3] and M de la L Olvera[3]

[1] Centro de Ciencias Aplicadas y Desarrollo Tecnológico, CCADET-UNAM, Universidad Nacional Autónoma de México, Apartado Postal 70-186, México, DF, 04510, Mexico
[2] Instituto de Física, Universidad Nacional Autónoma de México, Apartado Postal 20-364, México, DF, 01000, Mexico
[3] Departamento de Ingeniería Eléctrica, CINVESTAV IPN, SEES, Apartado Postal 14740, México, DF, 07000, Mexico

E-mail: omarm@aleph.cinstrum.unam.mx (O G Morales-Saavedra)

Received 23 February 2006, in final form 20 April 2006
Published 19 May 2006
Online at stacks.iop.org/JPhysCM/18/5105

Abstract

Chemically sprayed indium-doped zinc oxide thin films (ZnO:In) were deposited on glass substrates starting from zinc pentanedionate and indium sulfate. The influence of both the dopant concentration in the starting solution and the substrate temperature on the transport, morphology, composition, linear and nonlinear optical (NLO) properties of the ZnO:In thin films were studied. The structure of all the ZnO:In thin films was polycrystalline, and variation in the preferential growth with the indium content in the solution was observed: from an initial (002) growth in films with low In content, switching to a predominance of (101) planes for intermediate dopant regime, and finally turning to a (100) growth for heavily doped films. The crystallite size was found to decrease with doping concentration and range from 36 to 23 nm. The film composition and the dopant concentration were determined by Rutherford backscattering spectrometry; these results showed that the films are almost stoichiometric ZnO. The optimum deposition conditions leading to conductive and transparent ZnO:In thin films were also found. In this way a resistivity of 4×10^{-3} Ω cm and an average transmittance in the visible spectra of 85%, with a (101) preferential growth, were obtained in optimized ZnO:In thin films.

(Some figures in this article are in colour only in the electronic version)

[4] Author to whom any correspondence should be addressed.

 © 2006 IOP Publishing Ltd Printed in the UK

1. Introduction

Zinc oxide (ZnO) in thin film form has received a renewed interest not only for the wide applications encountered in optoelectronic and sensing devices [1–5] but also, as has been pointed out by Kumar *et al* [6], for the device quality of the ZnO thin films developed on cheap glass substrates [7]. Although ZnO in thin film form obtained by physical techniques shows the best characteristics [8–10], it should be mentioned that under certain controlled conditions the development of quality films based on less expensive chemical techniques is also possible [11–13]. As a matter of fact, the chemical spray technique (CST) has emerged as an adequate process in the manufacturing of ZnO thin films with physical properties that match well with those obtained by means of high vacuum techniques. A lot of work based on the enhanced transport and optical properties of ZnO thin films deposited by the CST has been reported [14, 15]. The CST being a well-established technique to produce high quality films, we are interested in the contributions based on the deposition variations that lead to films with enhanced properties.

In the manufacturing of transparent electrodes, one of the most successful results reached up to now has been the incorporation of indium (In) as impurity into the ZnO lattice, as no post-annealing treatment in a reducing or vacuum environment is required in order to obtain low resistivity values, of the order of 10^{-3} Ω cm [16]. It is worth mentioning that according to the professional literature, ZnO thin films are usually obtained starting from zinc acetate and indium chloride. However, as has been demonstrated by Smith *et al* [17], the properties of ZnO thin films can be dramatically affected by variations in the solvents used. As a consequence, it can be expected that differences in the physical properties of chemically sprayed ZnO thin films can be found when the Zn and In reactants are varied. Works based on the CST do not report zinc pentanedionate as well as indium sulfate as starting compounds in the deposition of ZnO thin films. In addition, to our best knowledge not only is there very little information concerning luminescent properties but also no data concerning the nonlinear optical properties of chemically sprayed ZnO:In thin films are encountered in the professional literature.

In the present work, the effect of indium doping on the composition, morphological, transport and optical properties of zinc oxide thin films deposited on sodocalcic glass substrates using a spray pyrolysis technique, starting from zinc pentanedionate and indium sulfate, is presented. In addition the quadratic nonlinear optical response $\chi^{(2)}$ of ZnO:In thin films is evaluated for the first time.

2. Experimental procedure

ZnO:In thin films were obtained from a solution containing zinc (II) pentanedionate [$Zn(C_5H_7O_2)_2{\cdot}H_2O$] (from Alfa) dissolved in a mix of deionized water, acetic acid [CH_3CO_2H] (from Baker) and methanol [CH_3OH] (from Baker) (volume proportion of 125:50:320, respectively) at 0.2 M. Indium (III) sulfate [$In_2(SO_4)_3$] (from Alfa) was used as the dopant source; the percentage atomic ratio of indium with respect to zinc in solution, [In]/[Zn], was used as the reference of the doping level in this work. The atomic percentage values studied were 1, 2, 4, 6 and 10 at.%. The films were deposited on sodocalcic glass substrates, carefully cleaned prior to deposition. The substrates were then placed on a fused tin bath, whose temperature was measured just below the substrate using a thin chromel–alumel thermocouple contained in a stainless steel metal jacket. The substrate temperature varied from 425 to 500 °C in steps of 25 °C. The solution and nitrogen gas flow used in this work were 12 ml min^{-1} and 8 L min^{-1}, respectively.

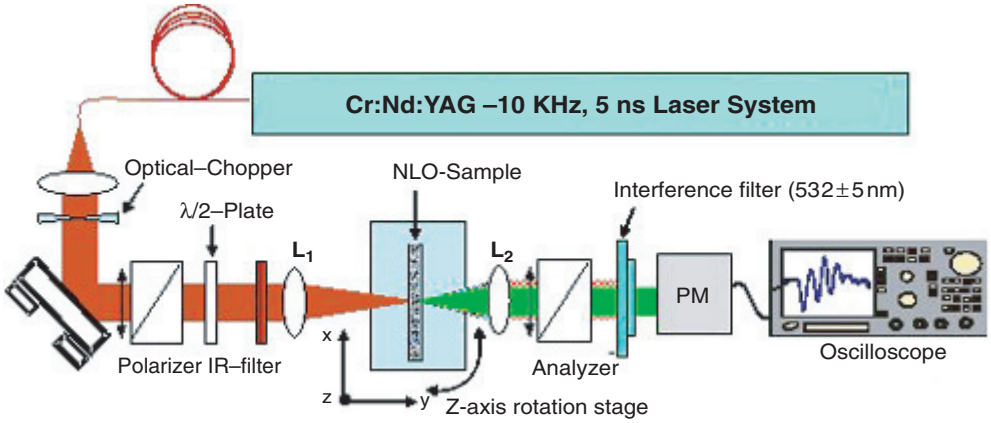

Figure 1. Experimental set-up for SHG measurements in ZnO:In thin films.

The electrical sheet resistance of all the samples was measured by the conventional four-aligned probe method (Veeco equipment) with the appropriate correction factors. The microcrystalline structure was determined through x-ray diffraction with the θ–2θ technique on a Siemens D5000-diffractometer using Cu Kα_1 ($\lambda = 0.154\,05$ nm) radiation. The morphology of the films was studied by scanning electron microscopy (SEM) in an LV JEOL 5600 electron microscope and atomic force microscopy (AFM) (Park AutoProbe CP equipment). In the last case, the deposited samples were analysed in contact mode using a Si Ultralever^{TM} tip with an applied force of 0.05 N m^{-1}, and a resonant frequency of 22 kHz. The applied force on the surface was of the order of 0.8 nN. Optical transmittance spectra of the films in the range from 200 to 1000 nm were obtained with a double-beam spectrophotometer (Shimadzu UV–VIS model 260), taking air as the reference.

The photoluminescence (PL) spectra of selected samples were obtained from 340 to 900 nm using an excitation line at $\lambda_{exc} = 300$ nm (FluoroMax-3, Jobin–Yvon–Horiba). Selected samples were also studied as active media for second harmonic generation (SHG). Measurements were taken at room temperature. Figure 1 depicts the implemented SHG set-up. A commercial diode pumped passive Q-switched Cr:Nd:YAG Laser system, operating at $\lambda_\omega = 1064$ nm with a repetition rate of 10–12 kHz and a pulse width of $\tau = 7$ ns (Smart Laser Systems, SLS-Berlin), was implemented to provide the fundamental wave. Typical pulse powers of 120 μJ were integrated through the windows of an optical chopper (50 Hz) in order to irradiate the samples with a variable intensity ranging from 60 to 80 MW cm^{-2}. The samples showed high threshold values to laser induced damage, making the use of neutral density filters unnecessary. It was possible to select the desired polarization of the fundamental beam by means of an IR-coated Glan–Taylor polarizer and a quartz retarded ($\lambda/2$-plate). A second polarizer was used as analyser, allowing the characterization of the SHG light. The second harmonic wave ($\lambda_{2\omega} = 532$ nm) was detected by a sensitive photomultiplier tube (HAMAMATSU, R-928) behind interferential optical filters centred at 532 ± 5 nm. The SHG device was calibrated by means of a Y-cut α-quartz crystal wedged in the $\chi_{11}^{(2)}$-direction (0.64 pm V^{-1}), which is frequently used as a nonlinear optical (NLO) reference standard via the Maker-Fringes method [18 p. 66] [19–22].

3.1 MeV ^{4}He Rutherford backscattering spectrometry (RBS) was used to determine the elemental composition of the ZnO films. In particular, with a ^{4}He beam we can take advantage of the elastic $^{16}O(\alpha,\alpha)^{16}O$ scattering resonance at 3.045 MeV for the oxygen

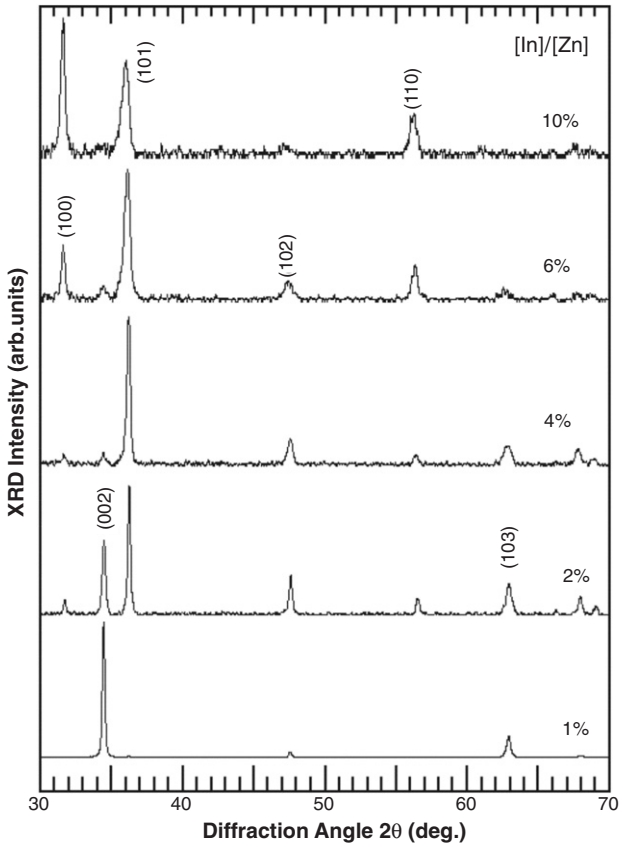

Figure 2. X-ray diffraction patterns of In-doped ZnO thin films deposited at 475 °C at different indium concentrations in the starting solution.

measurements [23]. At this resonant energy, the cross-section for oxygen is 25 times larger than its corresponding Rutherford cross-section, allowing high sensitivity for oxygen content determination [24]. The film composition was then determined by fitting the experimental RBS spectra using the RUMP simulation program [25]. These experiments were performed using the 3 MV Tandem Accelerator (NEC 9SDH-2 Pelletron) at the Instituto de Física (Universidad Nacional Autónoma de México, UNAM).

3. Results and discussions

3.1. Structure and morphology

X-ray diffraction (XRD) pattern studies revealed that all the films exhibited a polycrystalline arrangement, fitting well with the hexagonal ZnO structure [26]. The XRD patterns of ZnO:In thin films deposited at distinct [In]/[Zn] ratios in the starting solution and at $T_S = 475\,^{\circ}\mathrm{C}$ are shown in figure 2. The variation in the [In]/[Zn] rate in the solution changes the intensity of the peaks. In fact, the films deposited with a doping level of [In]/[Zn] = 1 at.% show that the signal associated with the (002) planes prevails over the other signals. In the case of the films doped with a ratio of [In]/[Zn] = 2 at.%, a change from (002) to (101) is observed, whereas

Table 1. Preferentially oriented planes and crystallite size variations of ZnO films as a function of the doping concentrations.

Dopant concentration (at.%)	Plane	Crystallite size (nm)
1	(002)	35.74
2	(101)	34.82
4	(101)	29.34
6	(101)	26.22
10	(100)	22.89

for films deposited with a doping level of 4 and 6 at.%, both the (101) and (100) peaks increase at the expense of the (002) signal. Finally, a preferential (100) growth is observed in the ZnO:In thin films deposited with a solution containing a dopant level of 10 at.%. The evolution of the preferential growth is consistent with the fact that undoped ZnO thin films deposited by the CST display a preferential (002) growth [27]. In the case of a low doping level, the In ions incorporated into the lattice do not markedly affect the (002) growth. In an intermediate doping regime, where the solubility limit of indium in ZnO is reached, the effect of the In ions on preferential growth is apparent, as planes other than (002) are favoured. As a matter of fact, Smith *et al* [17] have explained how acid variations dramatically affect the film morphology of ZnO thin films deposited by the Pyrosol technique.

The crystallite size was estimated using the (101), (002) and (100) diffraction peaks from the XRD data in accordance with the Debye–Scherer formula [28]:

$$D = \frac{9\lambda}{B\cos\theta}, \tag{1}$$

where D is the crystallite size in nanometres, λ is the wavelength value of the Cu Kα_1 line, θ is the Bragg diffraction angle and B is the FWHM of the diffraction peak measured in radians. The results are listed in table 1. According to these results, the crystallite size of the ZnO:In thin films decreases from 36 to 23 nm as the doping concentration in the solution increases from 1 to 10 at.%.

3.2. Electrical properties

The variation in the resistivity of the ZnO:In thin films as a function of both the [In]/[Zn] ratio in the solution and the substrate temperature T_S is shown in figure 3. It is evident that for a fixed T_S, as the In concentration in the solution increases, the resistivity of the ZnO:In thin films decreases, reaching a minimum value depending on the T_S. Further increase in the [In]/[Zn] value in the solution leads to an increase in the resistivity values of the ZnO:In thin films. Concerning the effect of the substrate temperature, a similar trend is observed: the resistivity of the ZnO:In thin films decreases with increasing T_S, again reaching a minimum value, and then it increases with a further increase in the T_S values. The lowest resistivity value is of the order of 4.1×10^{-3} Ω cm for ZnO:In thin films deposited with a dopant content of [In]/[Zn] = 6 at.%, within the 450–475 °C interval. These results are in good agreement with some other previous published data concerning chemically sprayed ZnO:In thin films deposited from zinc acetate and indium chloride [29]. The role of the indium concentration in the solution is explained on the basis of the gradual substitution into the Zn sites by In^{3+} ions, reaching the solubility limit in the ZnO lattice (of the order of 6 at.%), where the optimum value of the resistivity is found. A further increase in the indium concentration leads to a segregation of the In from the bulk to the grain boundaries, causing an increase in the resistivity values of the ZnO:In thin films [30]. On the other hand, the substrate temperature affects mainly the reaction formation process

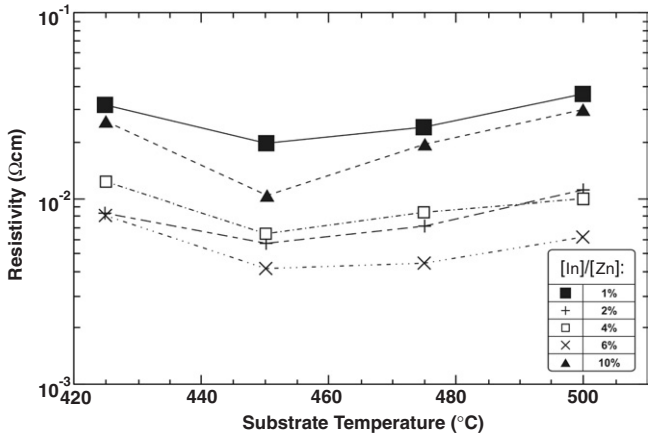

Figure 3. Electrical resistivity as a function of the [In]/[Zn] concentration in the starting solution, for ZnO:In films deposited at different substrate temperatures.

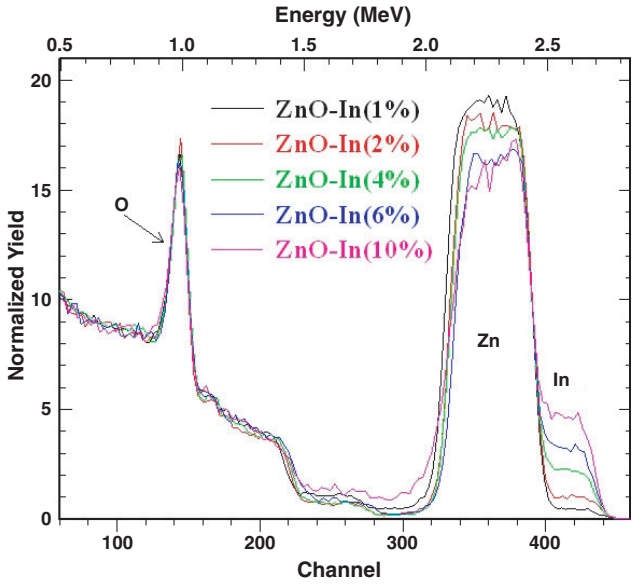

Figure 4. Experimental RBS spectra obtained with a 3.1 MeV $^4He^+$ beam from the ZnO:In films deposited at 475 °C at different indium concentrations in the starting solution.

of ZnO, as the heterogeneous reaction between reactants and surface is activated only by the thermal energy [11]. In what follows we will focus on the properties of the films deposited under optimized conditions.

3.3. Film composition and doping concentration

Figure 4 shows the experimental RBS spectra, obtained with a 3.1 MeV ^{4}He beam, of the ZnO:In thin films with different [In]/[Zn] ratios in the starting solution and deposited at $T_S = 475$ °C. One can clearly observe that the contribution of In to the RBS spectrum increases

Table 2. Oxygen and indium atomic concentrations normalized as $Zn_1O_xIn_y$ for the different substrate temperatures. The film thickness determined from RBS studies is expressed in areal density units (1×10^{15} atoms cm^{-2}), but length units are also included. Thickness (cm) = $N(1 \times 10^{15}$ atoms cm$^{-2}) \times A$ (g)/ρ (g cm$^{-3}) \times N_{Av}$, where N is the areal density, A the atomic weight of ZnO, $\rho = 5.6$ g cm^{-3} its density, and $N_{Av} = 6.02 \times 10^{23}$ the Avogadro number.

Nominal doping (at.%)	Thickness RBS (1×10^{15} atoms cm^{-2})	Thickness (nm)	Oxygen O_x	Indium In_y
1	3350	400	0.95	0.011
2	3200	385	1.05	0.022
4	3200	380	1.05	0.048
6	2900	350	1.1	0.073
10	3100	375	1.0	0.11

as a function of the doping concentration in the solution. The simulation of the RBS spectra reveals that our films are almost stoichiometric, with a composition close to ZnO, as indicated in table 2. Moreover, the RBS results show that the In doping concentrations in our films are proportional to the [In]/[Zn] ratio in the starting solution. In fact, the y content of indium in the $Zn_1O_1In_y$ films ranges from $y = 0.011$ to 0.11 for the ZnO:In thin films film deposited using a doping level of 1 and 10 at.% in solution, respectively, as shown in table 2. This exhibits a clear correlation between the doping level in the starting solution and the indium content determined by RBS.

3.4. AFM and SEM morphological results

Atomic force micrographs of the two- and three-dimensional surface morphology of ZnO:In thin films deposited with three different [In]/[Zn] ratios in the solution, namely 1, 6 and 10 at.%, are shown in figures 5(a)–(c) (2D) and in figures 5(d)–(f) (3D), respectively. In the case of the ZnO:In films deposited with a doping level of [In]/[Zn] = 1 at.% in solution, the surface is covered by grains with a narrow grain size distribution and a rounded (in some cases almost triangular-shaped) geometry. From amplified high-quality digitalized images, an average grain size of the order of 0.11 μm was measured. Further increase in the [In]/[Zn] ratio in the solution, in the range from 2 to 4 at.%, makes the corresponding morphology (not shown here) become smoother, with a smaller grain size. In the case of the films deposited with an [In]/[Zn] ratio of 6 at.%, changes to flake-like and triangular-shaped grains with a wider grain size distribution, ranging from 0.1 to 0.2 μm, occur, as is shown in figure 5(b). Finally, the films deposited with a ratio of 10 at.% exhibit the formation of a porous structure with larger grains, and a wider distribution in the grain size, as is shown in figure 5(c).

The root-mean-square (rms) roughness of the samples deposited with solutions containing [In]/[Zn] ratios of 1 and 10 at.% were 10.7 and 40.5 nm, respectively, showing that as the [In]/[Zn] concentration in the solution increases, the corresponding roughness of the ZnO:In thin films also increases. This tendency shows that the growth process is affected by the increase of the doping level in the starting solution, suggesting that the surface mobility of the reactants on the surface can be affected in such a way that worse accommodation, and hence an uneven surface, occurs as the [In]/[Zn] ratios increase.

Figures 6(a)–(e) show the morphology variations of ZnO:In thin films as seen in scanning electron microscopy as a function of the [In]/[Zn] content and deposited at $T_S = 475\,^{\circ}$C. In figure 6(a) ([In]/[Zn] = 1 at.%) a uniform and regular surface with almost null porosity and a monomodal grain size distribution can be observed everywhere. In figure 6(b) ([In]/[Zn] = 2 at.%) a rounded surface configuration can be observed, this texture is formed after the collision of a drop of solution onto the substrate, this last arrangement shows a uniform

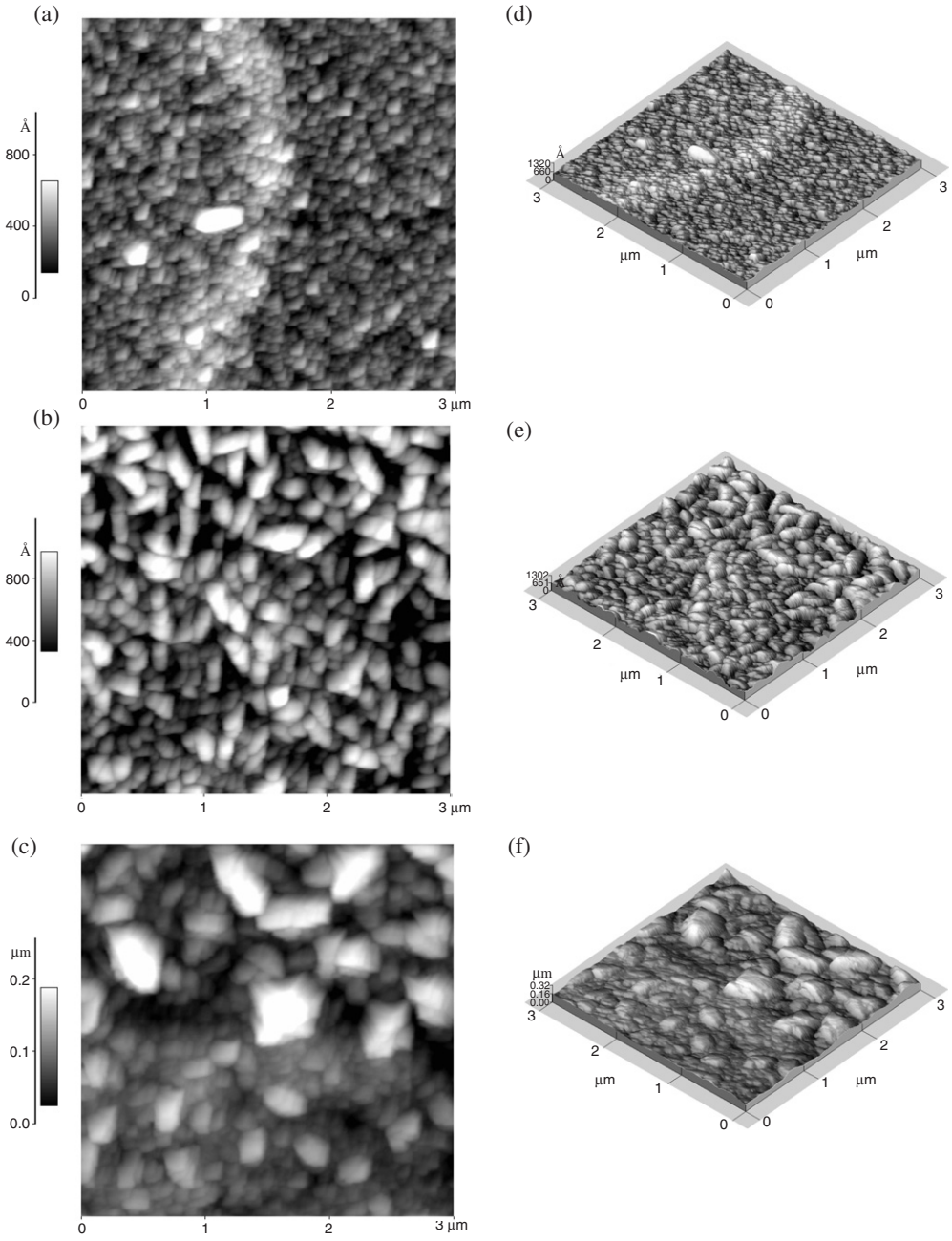

Figure 5. Bidimensional (2D) and tridimensional (3D) micrographs obtained with atomic force microscopy, showing the surface morphology of ZnO:In thin films deposited at 475 °C with different indium concentration in the starting solution: (a, d) 1 at.%, (b, e) 6 at.%, and (c, f) 10 at.%.

surface and a low inter-grain porosity. Here, at least a bimodal grain size distribution can be noticed. In figure 6(c) ([In]/[Zn] = 4 at.%) noticeable changes in the surface configuration with respect to the ones presented in figures 6(a) and (b) can be observed: the density of the surface increases and the grain size distribution becomes smaller. In figure 6(d)

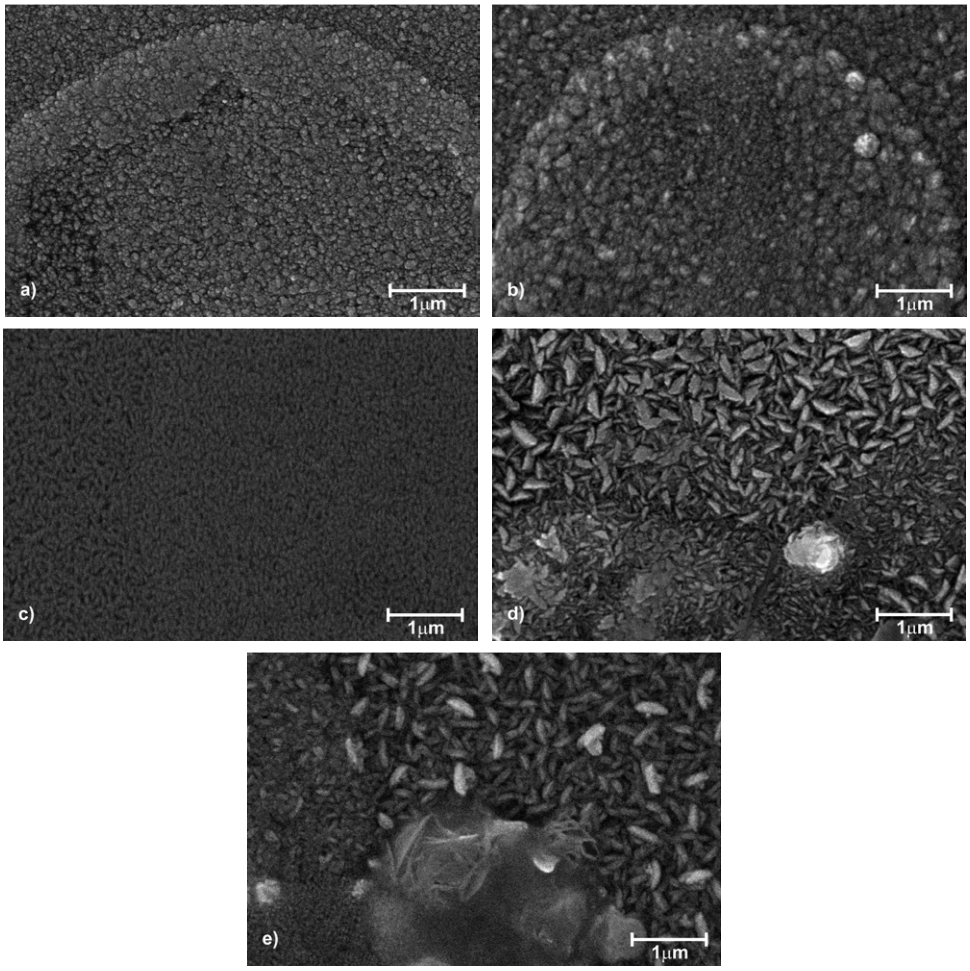

Figure 6. SEM micrographs of ZnO:In thin films deposited at 475 °C with different indium concentration in the starting solution: (a) 1 at.%, (b) 2 at.%, (c) 4 at.%, (d) 6 at.%, and (e) 10 at.%.

([In]/[Zn] = 6 at.%), the grains present a randomly oriented flake-like configuration with two different grain sizes and the intergranular space is clearly increased. In figure 6(e) ([In]/[Zn] = 10 at.%) a similar configuration of flake-like large grains together with very small grains densely aggregated is obtained. The influence of In content in the surface structural configuration of the ZnO:In thin films is clearly appreciated in the SEM micrographs, and it is expected that this behaviour will affect other physical properties, as will be shown later. It is worth mentioning that similar flake configurations were reported by Young and Lee [31] in Al-doped ZnO, and they attributed the configuration to pH variations. Yamada *et al* also reported similar configurations in textured ZnO:In films [32].

3.5. Optical properties

The optical transmittance spectra of ZnO:In thin films deposited with solutions whose [In]/[Zn] ratios were 1, 2, 4, 6 and 10 at.%, and which were deposited at $T_S = 475\,^{\circ}\mathrm{C}$, are shown in figure 7. It is evident from this figure that as the [In]/[Zn] ratio in the solution increases, the

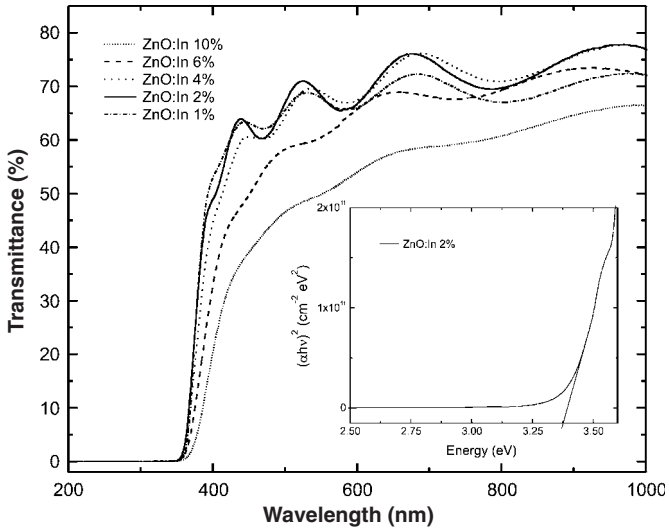

Figure 7. Optical transmittance spectra for ZnO:In thin films deposited at 475 °C with different concentrations in the starting solution. The inset show the calculation technique used to estimate the E_g values.

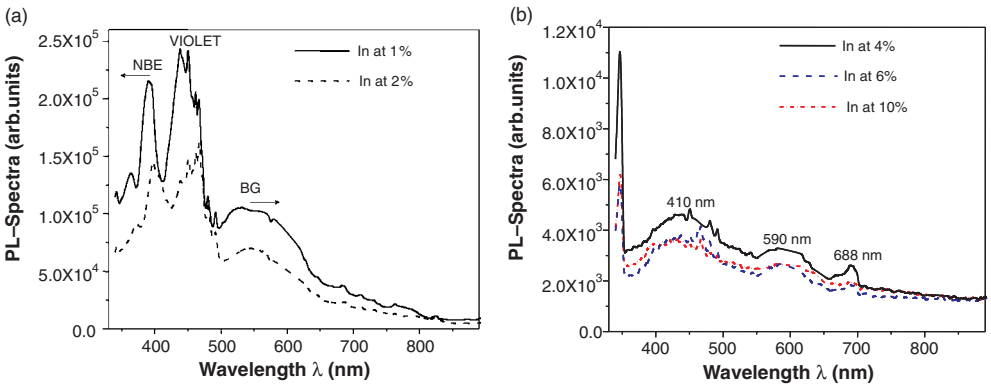

Figure 8. Photoluminescence spectra of typical indium-doped zinc oxide thin films deposited at $T_S = 475$ °C (excitation at $\lambda = 300$ nm), with different indium concentration in the starting solution, (a) and (b).

corresponding transmittance of the ZnO:In thin films decreases. The increase in the dopant concentration causes the amplitude of the fringe pattern to become smaller and finally become flat for the samples deposited with a 10 at.% [In]/[Zn] ratio. The inset in figure 7 shows a typical plot of $(\alpha h\nu)^2$ as a function of $h\nu$, where α is the optical absorption coefficient, and $h\nu$ is the energy of the incident photons. From these curves we can estimate the optical band gap (E_g) values, by the extrapolation of straight line to $(\alpha h\nu)^2 = 0$, as shown in the inset of figure 7. It was found that the value of E_g is slightly increased (3.40 eV) with the dopant concentration of 4 at.% and it begins to decrease (3.27 eV) until reaching the concentration of 10 at.%.

The PL spectra of the samples deposited with several [In]/[Zn] ratios in the solution, namely from 1 to 10 at.%, at 475 °C, are shown in figure 8 (the excitation wavelength was set to

$\lambda_{exc} = 300$ nm). In general, the lightly doped samples (1 and 2 at.% In, see figure 8(a)) reveal strong PL activity, whereas the heavily doped samples (4, 6 and 10 at.% In, see figure 8(b)) show a weaker PL emission. A complex structure conformed by several emission bands can be analysed from these experiments: the characteristic blue-green (BG) emission band (broad fluorescence band, main peak centred at 524 nm), typically observed in undoped ZnO samples, can be first recognized. In our case, however, the BG-emission band of ZnO:In films was found to be slightly narrower (480–630 nm, main peak range: 512–536 nm) and considerably weaker than that observed for pure ZnO and doped ZnO:F samples [14, 33–35]. Nevertheless, the centre responsible for such emissions has not yet been completely understood. In a recent report, it was established that the origin of the BG emissions might be due to the transition from the conduction band to the O_{Zn} level [34]. Incorporation of indium apparently resulted in a competitive phenomenon that overshadows the BG emission observed in ZnO samples, diminishing then the intensity of the main BG peak. Moreover, In-doped samples exhibit other interesting and dominant PL bands: an intense and broad violet band (406–470 nm) and a well defined UV emission band (340–390 nm), corresponding to the near band-edge (NBE) emission.

The BG, violet and NBE emissions depend drastically on the In content in the starting solution, and show a complex behaviour described as follows: for increasing In concentrations, the BG emission is red-shifted (band-shift tendencies are indicated by small arrows in figure 8) and drastically attenuated: the main peak is centred at 590 nm (10 at.% In); this emission may be due to the localized state introduced by the indium impurities [36]. On the other hand, the UV emission is shifted to lower wavelengths but the PL intensity was not dramatically affected. From the optical absorption spectra, one can identify for heavy doped samples that the peak position of the NBE or UV emission agrees well with the value of absorption edge. NBE emission at low temperature is well understood, owing to the sharp and intense emission peaks [35], but the observed band-shift might be related to the nature of variation of the band gap. Furthermore, attenuation of the PL intensity observed for the violet and NBE emissions with doping concentration might still be related to crystallinity, since the violet emission is probably due to the radiative defects related to the interface traps existing at the grain boundaries and emitted from the radiative transition between this level and the valence band [6, 34, 37, 38]. Kumar *et al* [6, 34] observed very recently many of the features discussed here, but contrary to our results, an opposite band-shift was observed in both the NBE and BG emission bands; the exact mechanism responsible for this differing behaviour is still not yet clearly understood. The other two peaks (at 410 and 688 nm) identified by Kumar *et al* can be also recognized in our experiments for heavily In-doped ZnO samples. The peak at 410 nm corresponds to the violet emission and lies within the 406–470 nm emission band measured in our experiments. Finally, the peak at 688 nm might be due to emission from a level caused by oxygen interstitials [34, 37, 38]. Even though it was not due to doping, we were not able to observe this emission for undoped and fluorine-doped ZnO samples [33], where the very high intensity of BG emission may annul this peak. Indium doping caused weakening of BG emission, and hence the emission at 688 nm becomes more prominent.

The possibility for obtaining NLO properties such as SHG by irradiation of the ZnO:In samples with the standard wavelength of a YAG laser system through the $\chi^{(2)}$ nonlinear optical response was also studied in this work. Moderated SHG intensities were detected at room temperature in the far field for ZnO:In thin films doped with 1, 2 and 4 at.% In, whereas the samples having 6 and 10 at.% In showed negligible SHG. The SHG signals, detected using a line-interferential filter (532 ± 5 nm) and a sensitive photomultiplier tube placed behind a fine optical collimator system, demonstrate that the detected irradiation was in fact the doubled frequency of the fundamental wave targeted to the ZnO:In samples. Figure 9(a) shows the

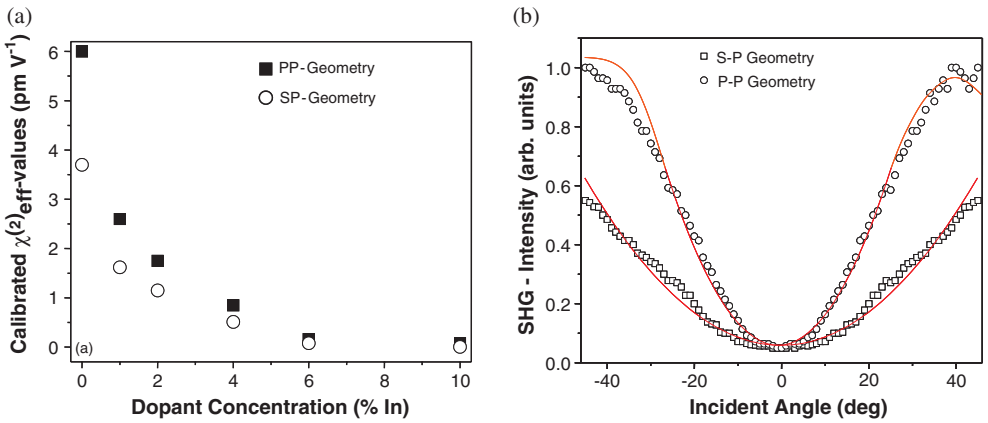

Figure 9. (a) Calibrated nonlinear $\chi^{(2)}_{\rm eff}$-coefficients of indium-doped zinc oxide thin film layers deposited at $T_{\rm S} = 450\,^{\circ}$C, with different indium concentration in the starting solution; measurements were performed for P–P and S–P polarization geometries. (b) Angle-dependent SHG measurement performed in the (1 at.% In) sample (solid line: theoretical fit).

nonlinear optical response of selected samples (including an undoped ZnO reference sample), where the calibrated nonlinear optical $\chi^{(2)}_{\rm eff}$-coefficients of each polycrystalline film deposited at $T_{\rm S} = 450\,^{\circ}$C are indicated. The measurements were performed implementing P–P and S–P polarization geometries. The SHG intensity detected by the S–P geometry was found to be about 30–40% weaker than that observed for the P–P configuration. A relative calibration of the SHG signal from the samples was performed following the standard Maker-Fringes method, implementing a Y-cut α-quartz crystal wedged in the $\chi^{(2)}_{11}$-direction, which is commonly used as a standard NLO reference. A simple equation allowed us to provide a first relative estimation for the nonlinear $\chi^{(2)}_{\rm eff}$-coefficients or effective second-order nonlinear optical susceptibility of the samples, by directly comparing the quadratic intensity dependence between the SHG signal of the reference crystal and that observed for the ZnO:In samples. Equation (2) represents this quadratic nonlinear optical dependence (thin film sample approximation):

$$I_{2\omega} \propto I_{\omega}^{2} \left(l_{\rm c}^{\rm Film} \chi_{\rm eff}^{(2)-{\rm Film}} \right)^{2} \sin^{2} \left[\frac{\pi l^{\rm Film}}{2 l_{\rm c}^{\rm Film}} \right], \tag{2}$$

where $l_{\rm c}^{\rm Film}$ represents the coherence length of the film sample and $l^{\rm Film}$ is the sample thickness. Note that for the present case the sample thickness is much smaller than the coherence length of the specimens (usually in the range of a few microns). Under this limit ($l^{\rm Film} \ll l_{\rm c}^{\rm Film}$) the relation between the generated SHG intensity and the intensity of the fundamental wave may be expressed as: $I_{2\omega} \propto I_{\omega}^{2}[(\pi/2) l^{\rm Film} \chi_{\rm eff}^{(2)-{\rm Film}}]^{2}$. This follows the NLO calibration using the reference crystal:

$$\chi_{\rm eff}^{(2)-{\rm ZnO:In}} \propto \chi_{11}^{(2)-{\rm Quartz}} \left(\frac{2 l_{\rm c}^{\rm Quartz}}{\pi l^{\rm Film}} \right) \left[\frac{I_{2\omega}^{\rm ZnO:In}}{I_{2\omega}^{\chi_{11}^{(2)}-{\rm Quartz}}} \right]^{1/2}, \tag{3}$$

where $l_{\rm c}^{\rm Quartz}$ is the coherence length of the quartz crystal ($\approx 22\ \mu$m) and $I_{2\omega}^{\chi_{11}^{(2)}-{\rm Quartz}}$ is the SHG intensity at maximum of the Maker-Fringes observed for the reference crystal.

The investigated samples show a clear dependence between the observed SHG intensity and the indium concentration: a huge decrement of the SHG signal is observed as the In content is lightly increased (see figure 9(a)). This fact should be directly related to the crystal structure,

domain sizes or film morphology achieved by increasing the amount of indium within the samples, as will be explained in more detail later. The existence of SHG for the lightly In-doped samples (1, 2 and 4 at.% In) reveals an average non-centrosymmetric structure of these crystalline thin films. However, the lack of SHG response observed in heavily indium-doped samples (6 and 10 at.% In), by angle-dependent SHG measurements (in both P–P and S–P polarization geometries), reveals the formation of a centrosymmetric crystalline arrangement or a polycrystalline structure with multiple variants, which might induce phase shifts that can lead to cross-cancellation of the SHG signals. As expected, no SHG arises from the glass substrates used in the NLO experiments.

So far, only SHG [39] and third-harmonic generation (THG) [40] have been reported for undoped ZnO thin film samples prepared by the metal–organic chemical vapour deposition technique (MOCVD) and the spin coating method, respectively. Recently we reported the SHG and THG of fluorine-doped ZnO thin film samples prepared by the CST method [33]. THG is possible, in principle, for all centrosymmetric materials; however, since pure ZnO has the hexagonal close packed (HCP) uniaxial non-centrosymmetric crystalline structure (6*mm* point group symmetry), SHG is allowed. We therefore investigated the SHG response of doped samples by the inclusion of indium ions. In fact, figure 9(a) presents, to our best knowledge, the first experimental observation of SHG for ZnO:In thin films deposited by a spray pyrolysis technique. The evaluated nonlinear $\chi^{(2)}_{\mathrm{eff}}$-coefficients for doped samples range from 0.004 to 2.6 pm V^{-1} (the maximal sensitivity of our experiments was of the order of 0.001 pm V^{-1}). For lowly In-doped specimens this value is an order of magnitude higher than the $\chi^{(2)}_{11}$-component of the reference crystal, and slightly smaller than the $\chi^{(2)}_{\mathrm{eff}}$-coefficient measured for an undoped ZnO reference sample. By considering the small thickness of our samples, these moderated SHG signals imply that the observed SHG originates from the bulk material rather than from surface effects, where only very weak SHG can be detected by lock-in amplification techniques. On the other hand, since SHG depends on the thickness of the sample, higher conversion efficiency must be expected for thicker (multilayer) samples, which could be promising for some nonlinear photonic and optoelectronic applications.

Due to small variations observed in the sample thickness (see table 2), the different effective second-order susceptibilities measured for ZnO:In thin films may come rather from different crystallinity. The decrement of the crystallite size with increasing indium concentration (see table 1) cannot explain the experimental results shown in figure 9(a) by assuming a high correlation between the morphological film structure and the NLO response [39]. In the last case, the vast number of grain boundaries or interfaces present for heavily indium-doped samples induces deviation of the atomic bonds between unitary cells from their equilibrium positions, which may cause dangling bonds resulting in extra carriers or defects in the film structure. This last fact, as has been previously demonstrated for ZnO and ZnO:F-based thin films, could enhance in principle the nonlinearity in crystals [33, 41, 42]. Since this dependence was not observed in our experimental results for In-doped ZnO films, it is then clear that the absence of SHG signal observed in heavily In-doped films is due to the variations of the crystalline lattices caused, in principle, by interstitial sites occupied by indium ions, which gradually deforms the symmetry of ZnO (see figure 2). Furthermore, the resistivity curves measured for In-doped ZnO samples can also partially explain the experimental results of figure 9(a): the decrease of the resistivity observed as the In doping increases to moderate values (1, 2 at.% In) indicates that the donor action of indium enhances the charge transfer between oxygen and zinc, which is a prerequisite for the existence of SHG activity. However, for higher doping levels, the resistivity values increase again and thus a decrease in the charge transfer and SHG response is observed. A similar behaviour between the resistivity and In doping concentration of ZnO thin films has recently been reported by Kumar *et al* [6, 34].

For these reasons, samples deposited at $T_S = 450\,^{\circ}C$ were chosen for SHG experiments, since the resistivity values for these samples were optimal for the observation of $\chi^{(2)}$ NLO effects, despite the fact that the crystalline structure and orientation strongly determine the SHG response.

Finally, due to the HCP structure and a preferential (002)-face growth, which is characteristic of ZnO in the wurzite form (zincite subgroup), the NLO $\chi^{(2)}$-tensorial properties of the ZnO:In (1 at.% In) sample were considered to be similar to that of an isotropic uniaxial medium. Hence, after considering Kleinman's symmetry condition, which requires that the involved frequencies in SHG experiments are far from resonances (see figure 7), the corresponding tensorial components of the second-order susceptibility were evaluated using angle-dependent SHG measurements (see figure 9(b)). For the 6*mm* symmetry corresponding to optically uniaxial media, only two independent nonzero coefficients can be evaluated: $\chi^{(2)}_{xzx} = \chi^{(2)}_{yzy} = \chi^{(2)}_{xxz} = \chi^{(2)}_{yyz} = \chi^{(2)}_{zxx} = \chi^{(2)}_{zyy}$ and $\chi^{(2)}_{zzz}$, which are commonly known as the $\chi^{(2)}_{31}$ and $\chi^{(2)}_{33}$ components in the contracted notation. The highest values for the ZnO:In (1 at.% In) sample of $\chi^{(2)}_{31} = 2.7$ pm V^{-1} and $\chi^{(2)}_{33} = 8.4$ pm V^{-1} were evaluated by theoretical fitting, according to the theory developed by Liu *et al* [39] and Cao *et al* [43], and agree well with the values obtained by the relative calibration performed with the Y-cut α-quartz crystal. The evaluated coefficients were found to be slightly smaller than those observed for ZnO:F thin films prepared under different substrates temperatures with the spray pyrolysis technique [33].

4. Conclusions

Highly conductive and transparent indium-doped zinc oxide thin films can be obtained by the spray pyrolysis technique starting from zinc pentanedionate and indium sulfate. The effect of the dopant level in the starting solution on the transport and structural properties of the films was established. The indium content in the solution affects the preferential growth and grain size distribution. Optimum films showing a minimum resistivity value of the order of $4.1 \times 10^{-3}\ \Omega$ cm, a transmittance of 85% and with a (101) preferential growth, were obtained from a solution with a dopant level of 6 at.% within an interval of T_S ranging from 450 to 475 °C. The physical characteristics of conductivity and transmittance of the ZnO:In thin films deposited with zinc pentanedionate and indium sulfate at least match with those of the corresponding films deposited starting from zinc acetate and indium chloride. The optical transmission spectra have a relatively high percentage of transmittance in the wavelength range from 400 to 900 nm. The optical band gap is of the order of 3.3 eV.

SHG studies have been performed in selected ZnO:In prepared samples (implementing both P–P and S–P polarization geometries). Observed SHG intensities were found to be drastically dependent on the In concentration as follows: a pronounced decrement in the SHG response was measured by increasing the In content. This last fact implies a strong crystalline rearrangement sensitively observed by NLO measurements. The highest $\chi^{(2)}_{\text{eff}}$-coefficient, found for the $T_S = 450\,^{\circ}C$ (1 at.% In) sample, shows a value of around 2.6 pm V^{-1} (P–P configuration). Finally, the components of the quadratic nonlinear susceptibility tensor were evaluated according to the HCP 6*mm* point group symmetry, distinctive of pure ZnO samples, by means of angle-dependent SHG measurements. Best theoretical fitting allowed us to estimate $\chi^{(2)}$-tensorial values of the order of $\chi^{(2)}_{31} = 2.7$ pm V^{-1} and $\chi^{(2)}_{33} = 8.4$ pm V^{-1}. Further studies on the deposition of ZnO:In films and optimization of the implemented CST parameters should be also performed in order to improve the NLO response of the samples and film quality.

Acknowledgments

We wish to thank A Palafox-Gómez, E-J Luna-Arredondo, M A Luna-Arias and A G López, for their technical assistance and contributions to film deposition and characterization. K López and F-J Jaimes are also acknowledged for the operation of the Tandem Accelerator. Two of the authors (O G Morales-Saavedra and A Maldonado) gratefully acknowledge the financial support of the CONACyT under project numbers 47421 and 42760, respectively. O G Morales-Saavedra also acknowledges financial support from the DAAD academic organization (Germany).

References

[1] Cooray N F Y, Kushiya K, Fujimaki A, Okumura D, Sato M, Ooshita M and Yamase O 1999 *Japan. J. Appl. Phys.* **38** 6213
[2] Segawa Y, Ohtomo A, Kawasaki M, Koinuma H, Tang Z K, Yu P and Wong G K L 1997 *Phys. Status Solidi* b **202** 669
[3] Lampert C M 1981 *Sol. Energy Mater.* **6** 1
[4] Jayadev D N, Sainkar S R, Karekar R N and Aiyer R C 1998 *Thin Solid Films* **325** 254
[5] Yoshino Y, Makino T, Katayama Y and Hata T 2000 *Vacuum* **59** 538
[6] Ratheesh Kumar P M, Sudha Kartha C and Vijayakumar K P 2005 *J. Appl. Phys.* **98** 023509
[7] Norton D P, Heo Y M, Ivill M P, Ip K, Pearton S J, Chisholm M F and Steiner T 2004 *Mater. Today* **7** 34
[8] Lee J H, Ko K H and Park J B O 2003 *J. Cryst. Growth* **247** 119
[9] Matsubara K, Fons P, Iwata K, Yamada A, Sakurai K, Tampo H and Niki S 2003 *Thin Solid Films* **431/432** 369
[10] Hamad O, Braunstein G, Patil H and Dhere N 2005 *Thin Solid Films* **489** 303
[11] Patil P S 1999 *Mater. Chem. Phys.* **59** 185
[12] Shishiyanu S T, Lupan O I, Monaico E V, Ursaki V V, Shishiyanu T S and Tiginyanu I M 2005 *Thin Solid Films* **488** 15
[13] Mahalingam T, John V S, Raja M, Su Y K and Sebastian P J 2005 *Sol. Energy Mater. Sol. Cells* **88** 227
[14] Ratheesh Kumar P M, Sudha Kartha C, Vijayakumar K P, Singh F and Avasthi D K 2005 *Mater. Sci. Eng.* B **117** 307
[15] El Hichou A, Addou M, Ebothé J and Troyon M 2005 *J. Lumin.* **113** 183
[16] Maldonado A, de la Olvera M L, Asomoza R and Tirado-Guerra S 2001 *J. Mater Sci.: Mater. Electron.* **12** 623
[17] Smith A and Rodríguez-Clemente R 1999 *Thin Solid Films* **345** 192
[18] Boyd R 1992 *Nonlinear Optics* (San Diego, CA: Academic) p 66
[19] Maker P D, Terhune R W, Nisenoff M and Savage C M 1992 *Phys. Rev. Lett.* **8** 21
[20] Zhang H Y, He X H, Shih Y H, Schurman M, Feng Z C and Stall R A 1996 *Appl. Phys. Lett.* **69** 2953
[21] Sanford N A, Davydov A V, Tsvetkovand D V, Dmitriev A V, Keller S, Mishra U K, Den Baars S P, Park S S, Han J Y and Molnar R J 2005 *J. Appl. Phys.* **97** 053512
[22] Gopalan V, Sanford N A, Aust J A, Kitamura K and Furukawa Y 2001 *Handbook of Advanced Electronic and Photonic Materials and Devices* vol 4 *Ferroelectrics and Dielectrics* ed H S Nalwa (New York: Academic) p 57
[23] Cameron J R 1953 *Phys. Rev.* **90** 839
[24] Vizkelethy G, Revesz P, Mayer J W and Li J 1993 *Surf. Interface Anal.* **20** 309
[25] Doolittle L R 1985 *Nucl. Instrum. Methods* B **9** 344
[26] *Powder Diffraction File, Data Card 5-644* 3c PDS International Center for Diffraction Data, Swartmore, PA
[27] Riad A S, Mahmoud S A and Ibrahim A A 2001 *Physica* B **296** 319
[28] Warren B E 1990 *X-Ray Diffraction* (New York: Dover) p 253
[29] Lee C, Lim K and Song J 1996 *Sol. Energy Mater. Sol. Cells* **43** 37
[30] Goyal D J, Agashe C, Takwale M G, Marathe B R and Bhide V G 1992 *J. Mater. Sci.* **27** 4705
[31] Ma T Y and Lee S C 2000 *J. Mater. Sci.: Mater. Electron.* **11** 305
[32] Yamada A, Fens W W, Konagai M and Takahashi K 1990 *Tech, Digest* vol I-PVSEC-5, Kyoto 1033
[33] Castañeda L, Morales-Saavedra O G, Acosta D R, Maldonado A and Olvera M de la L 2006 Structural, morphological, optical and nonlinear optical properties of fluorine-doped zinc oxide thin films deposited on glass substrates by the chemical spray technique *Phys. Status Solidi* a, at press (doi:10.1002/pssa.200521386)

[34] Kumar P M R, Kartha C S, Vijayakumar K P, Abe T, Kashiwaba Y, Singh F and Avasthi D K 2005 *Semicond. Sci. Technol.* **20** 120
[35] Klingshirn C 1975 *Phys. Status Solidi* b **71** 547
[36] Ortiz A, Falcony C, Hernández J A, Garcia M and Alonso J C 1997 *Thin Solid Films* **293** 103
[37] Jin B J, Im S and Lee S Y 2000 *Thin Solid Films* **366** 107
[38] Wang Y G, Lau S, Zhang X H, Lee H W and Tay B K 2003 *J. Cryst. Growth* **252** 265
[39] Liu C Y, Zhang B P, Binh N T and Segawa Y 2004 *Opt. Commun.* **237** 65
[40] Zhang L Z and Tang G Q 2004 *Opt. Mater.* **27** 217
[41] Khaled J, Fujiwara T, Ohama M and Ikushima A J 2000 *J. Appl. Phys.* **87** 2137
[42] Neuman U, Grunwald R, Griebener U and Steinmeyer G 2004 *Appl. Phys. Lett.* **84** 170
[43] Cao H, Wu J Y, Ong H C, Day J Y and Chang R P H 1998 *Appl. Phys. Lett.* **73** 572